Supporting Information

Customized Porous Aromatic Frameworks (PAFs) as an Oral Antidote for Efficient and Selective Intestinal Detoxification

Enpeng Xi, [†a] Yue Zhao, [†a] Huan Wang,[b] Yun Zhao,[a] Fangfang Cao,[*c] Yue Li,[*a] and Nan Gao[*a]

[a]Key Laboratory of Polyoxometalate and Reticular Material Chemistry of Ministry of Education and Faculty of Chemistry, Northeast Normal University, Changchun 130024, P. R. China

[b]Rehabilitation Department, Jilin Provincial Hospital of Chinese Medicine, Changchun 130021, P. R. China

[c]Key Laboratory of Big Data-Based Precision Medicine of Ministry of Industry and Information Technology, School of Engineering Medicine, Beihang University, Beijing, 100191, China

Corresponding Author: *Correspondence should be addressed to Fangfang Cao (fangfangcao@buaa.edu.cn), Yue Li (liy225@nenu.edu.cn), and Nan Gao (gaon320@nenu.edu.cn).

1. Experimental Procedures

1.1. Reagents and apparatus.

All chemicals and anhydrous solvents used in the experiments were purchased from commercial sources and used without any further purification. The monomers, catalysts, irinotecan hydrochloride, and SN-38 used for the synthesis of porous aromatic framework materials were purchased from Aladdin Reagent. Other reagents were purchased from Beijing Chemical institute. Infrared spectra were tested by a Nicolet-410 Fourier transform infrared spectrophotometer in the wavelength range of 4000 to 400 cm^{-1}. Powder X-ray diffraction data were performed on a Siemens D5005 diffractometer with a scan rate of 5 min $degree^{-1}$. Thermogravimetric analysis was measured on a Mettler Toledo thermal analyzer in the temperature range of 30-800 °C with a heating rate of 10 ℃ min^{-1}. Nitrogen adsorption-desorption isotherms were measured at 77 K on an Autosorb from 0 to 1 bar relative pressure. UV-visible absorption spectra were measured by a VARIAN Cary-60 UV-visible spectrophotometer in the wavelength range of 200-800 nm. ELISA tests were measured by an Infinite M Nano full-wavelength enzyme marker at 450 nm (reference wavelength 630 nm).

1.2 . High-Performance Liquid Chromatography.

Quantitative analysis of adsorbed drugs was performed using a high-performance liquid chromatography system (Agilent 1260 Infinity II). The column used was ZORBAX Eclipse XDB-C18 (50 mm × 4.6 mm, 5 μm). Mobile phase A consisted of aqueous solution containing 0.05% (v/v) formic acid, while phase B comprised acetonitrile solution containing 0.04% (v/v) formic acid. Linear gradient elution was employed with a total runtime of 4 minutes. The specific program was as follows: 0-3 minutes, phase A linearly decreased from 95% to 0%, phase B linearly increased from 5% to 100%; from 3 to 4 minutes, phase A remained at 0% and phase B at 100%. The flow rate was 3.5 mL/min. Column temperature was maintained at 30 °C. Detection wavelengths were 220 nm and 254 nm (using a diode array detector, DAD). The injection volume was 1.0 μL. Samples were diluted with methanol to a concentration of 0.1 mg/mL prior to injection and analysis.

1.3. Animals.

The mice (ICR) were purchased from Yisi Ltd (female, 6-8 weeks, weight 18-23 g). The animals were housed in groups (6 animals/cage) and all mice were maintained in a 12-hour light/dark cycle with temperature (24 ± 2 °C) and humidity (60 ± 5%) and provided with food and water randomly. All animal studies were conducted in accordance with the principles and procedures outlined in “Regulations for the Administration of Affairs Concerning Laboratory Animals”, approved by the National Council of China on October 31, 1988, and “The National

Regulation of China for Care and Use of Laboratory Animals", promulgated by the National Science and Technology Commission of China, on November 14, 1988. All animal studies were supervised by the Committee of Northeast Normal University Institutional Animal Care and Use.

1.4. Animal experiments.

A schematic design of the animal experiment is shown in Table S1. Two mice from each group were randomly selected for execution and dissected on days 9. The concentrations of the reagents used in the experiment were as follows CPT-11 injection was 10 mg mL^{-1} and the detoxifying agents was a suspension of 30 μg mL^{-1}. The irinotecan dosage for every mouse was 75 mg kg^{-1}, and the detoxifying agents was 200 mg kg^{-1}.

1.5. Histopathological analysis.

For histological analysis of colon tissue, small segments (1 cm) of the distal colon of mice from each study group were fixed with 10% paraformaldehyde at room temperature for 24 hours. Afterwards, the tissues were embedded in paraffin blocks. The tissues were sectioned at 4 μm thickness using a microtome and stained with hematoxylin-eosin (H&E) staining. Histological examination was performed using light microscopy. Microscopic sections of the colon were graded semi-quantitatively from 0 to 4 for the degree of inflammation and epithelial damage. The images were scored blindly.

1.6. Immunohistochemistry.

Colon sections were fixed in 10% paraformaldehyde and embedded in paraffin. Paraffin blocks were cut into 4-μm sections, dewaxed with xylene, and rehydrated with ethanol. After blocking for 1 hour, colon tissue was incubated with anti-mouse lymphatic vascular endothelial hyaluronan receptor 1 (LYVE-1) overnight at 4 °C. Sections were treated with an AEC substrate chromogenic agent to visualize the immune complexes. Immunohistochemical staining was observed under a light microscope. The density of Lyve-1 positive areas was observed at magnifications of ×10, ×20, ×40 using Slide Viewer software.

1.7. Determination of inflammatory factors.

Double antibody sandwich enzyme-linked immunosorbent assay (ELISA) was used to determine the levels of IL-6 and TNF-α in serum, strictly in accordance with the actual instructions.

1.8. Stability of PAF80-Z2-NH_3^+ under simulated GI conditions.

Stability studies were performed by suspending 30 mg of PAF80-Z2-NH_3^+ in 30 mL of the selected media (water, gastric, and intestinal). The suspensions were stirred under continuous stirring in an incubator at 60 rpm at 37 °C for 24 h. In order to recover the solid and liquid

phases, the suspensions were centrifuged at 14500 rpm for 10 minutes. PXRD analyses were performed to check their stability.

1.9. Hemocompatibility test.

The collected erythrocyte precipitate was repeatedly washed with PBS until it was observed as a colorless supernatant after centrifugation. 0.5 mL of 4% erythrocyte suspension was added to 0.5 mL of different concentrations of PAF80-Z2-NH_3^+ solution, making the final concentrations 10, 20, 30, 40, and 50 mg mL^{-1}. 0.5 mL of 4% erythrocyte suspension was then added to 0.5 mL of deionized water (positive control) and PBS (negative control), respectively. The absorbance of the supernatant obtained by centrifugation was measured at 540 nm.

1.10. H&E staining of major organs.

The main organ tissues of each group (heart, liver, spleen, lung, kidney) were stained with H&E, and the organs of each group were observed for organ damage.

1.10. Statistical processing.

Data were analyzed using SPSS 27 software, and the results of each group measurement were expressed as mean ± standard deviation ($x \pm S$), and one-way analysis of variance (ANOVA) was used for comparison between different groups. $p<0.05$ showed that the results were statistically different.

2. Results and Discussion

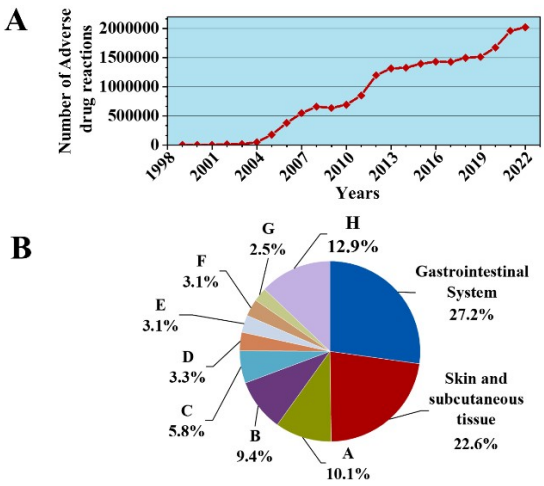

Fig. S1 (A) Growth trend of the number of reported ADRs from 1999 to 2022 in China. (B) The organs involved in ADR in 2022. The letters A to H represent systemic and sites of drug administration, nervous system, examination, respiratory system, heart organs, blood and lymphatic system, blood vessels and lymphatic vessels and others, respectively.

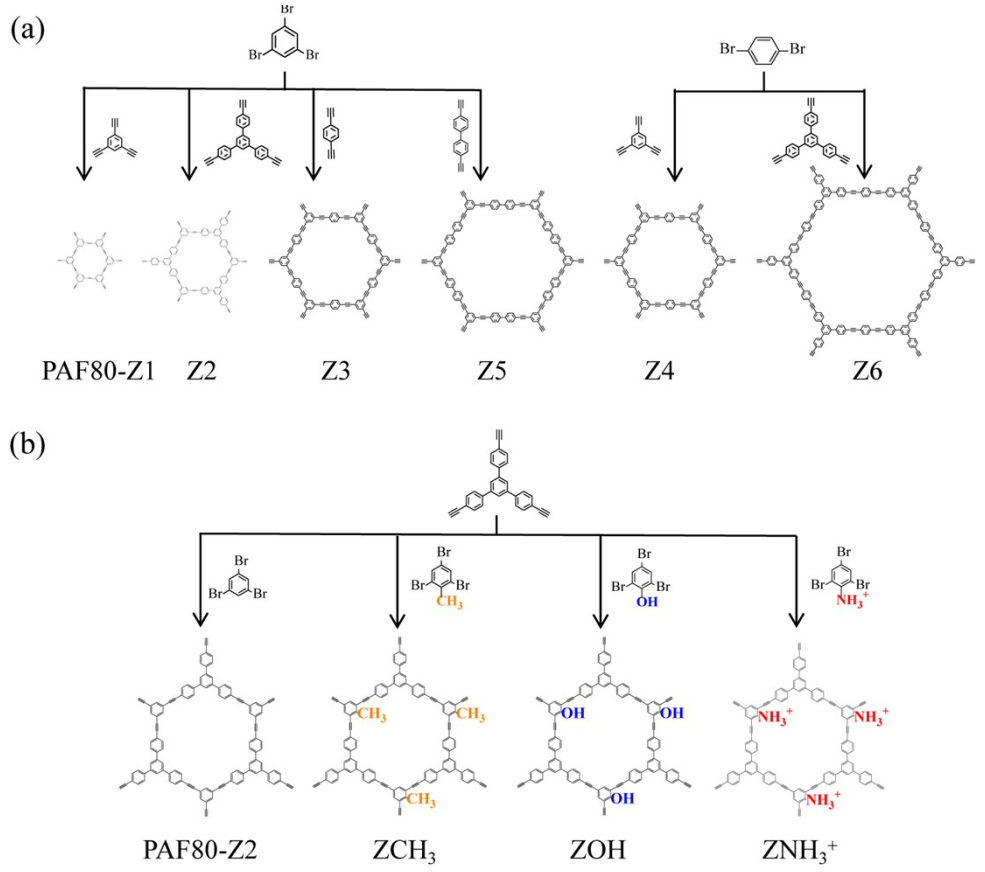

Fig. S2 (a) Schematic design of the structure of the PAFs material series (PAF80-Z1, Z2, Z3, Z4, Z5, Z6), (b) Schematic design of the structure of the PAFs material series (PAF80-Z2-CH_3, PAF80-Z2-OH and PAF80-Z2-NH_3^+).

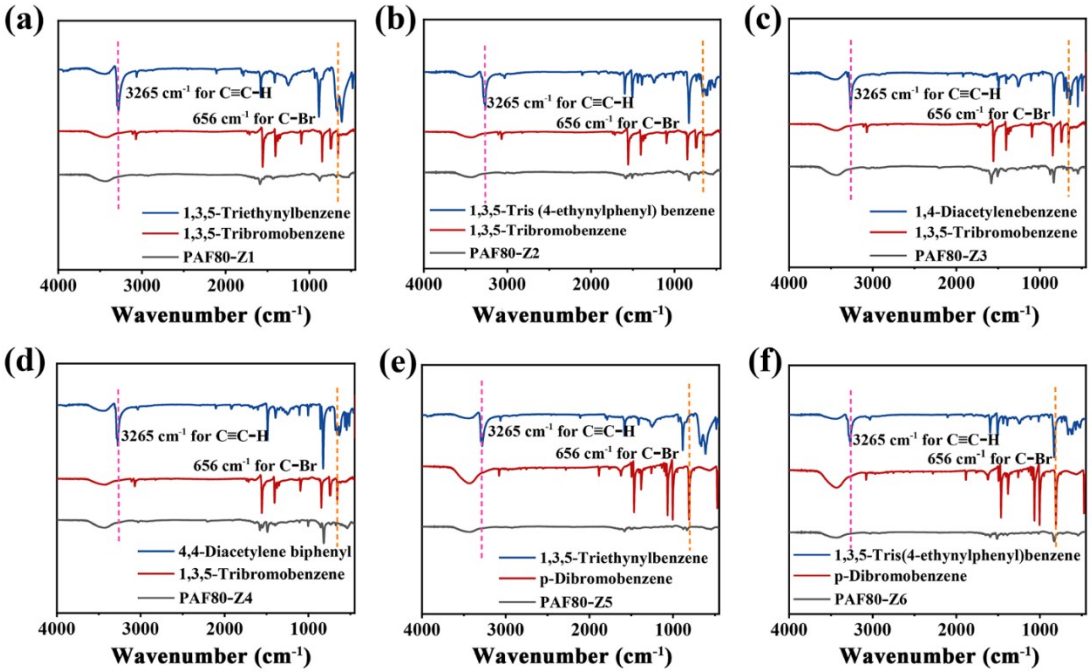

Fig. S3 FT-IR spectra of PAF80-Z1-Z6. The sharp peak located at 3265 cm^{-1} belongs to the stretching vibration of alkyne hydrogen in the structural unit containing acetylene functional group, and the absorption peak near 656 cm^{-1} is the stretching vibration of C-Br in the monomer, and the disappearance of these characteristic peaks proves that the monomer has completely disappeared and the reaction is complete.

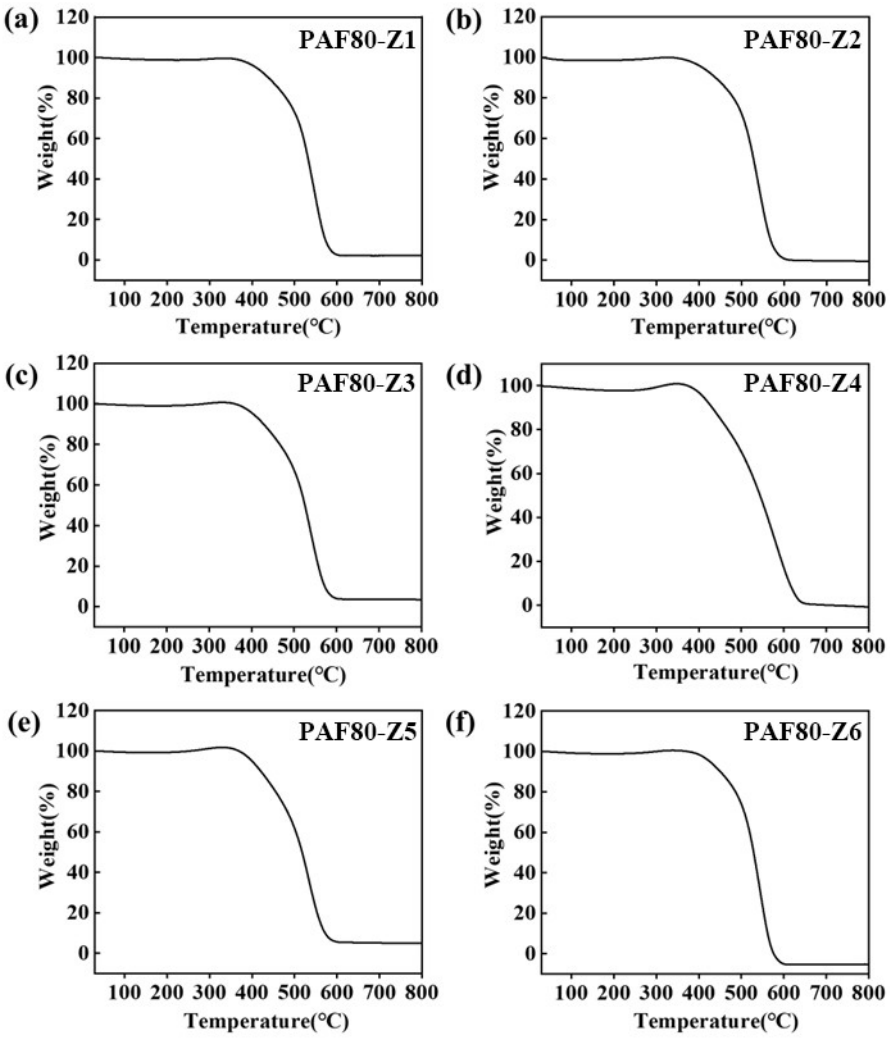

Fig. S4 TGA curves of PAF80-Z1-Z6. The thermal stability of the synthesized PAF materials was up to 400 °C, and no residues were observed above 800 °C.

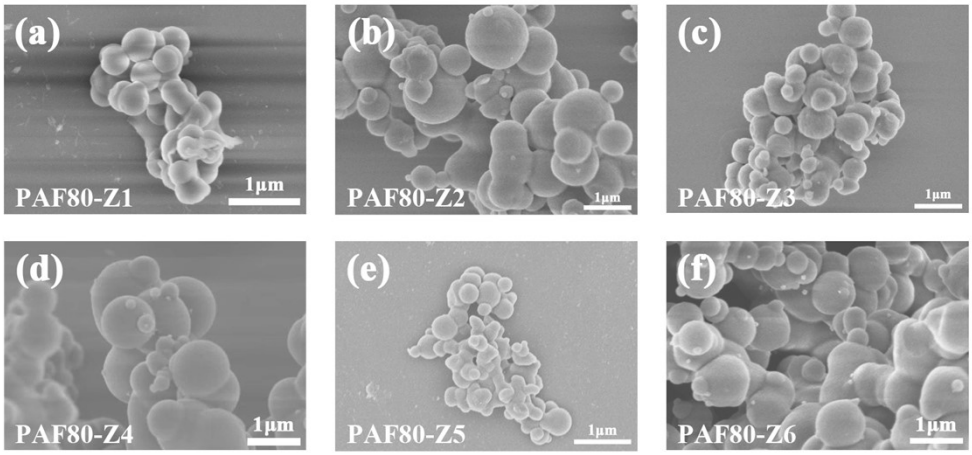

Fig. S5 SEM images of PAF80-Z1-Z6. The morphology of the material is submicron particles and spherical distribution.

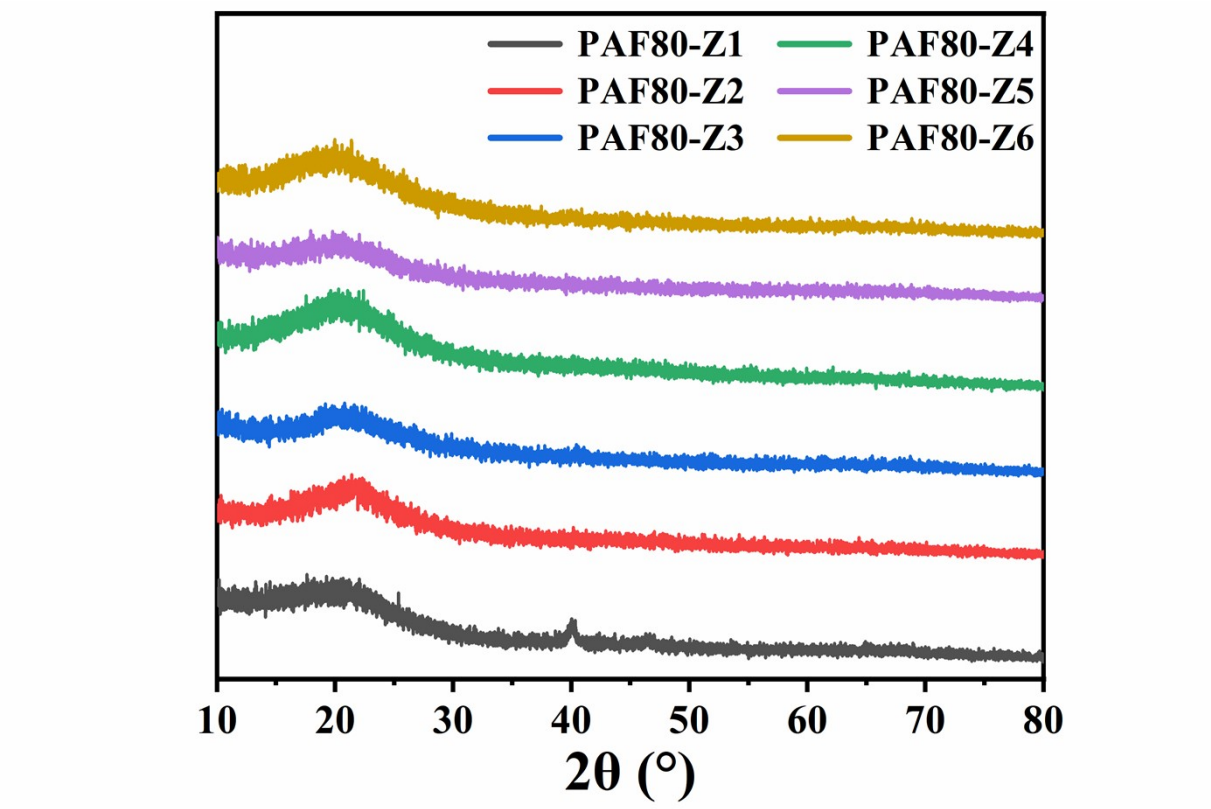

Fig. S6 PXRD patterns of PAF80-Z1 (black curve), Z2 (red curve), Z3 (blue curve), Z4 (green curve), Z5 (purple curve), Z6 (brown curve).

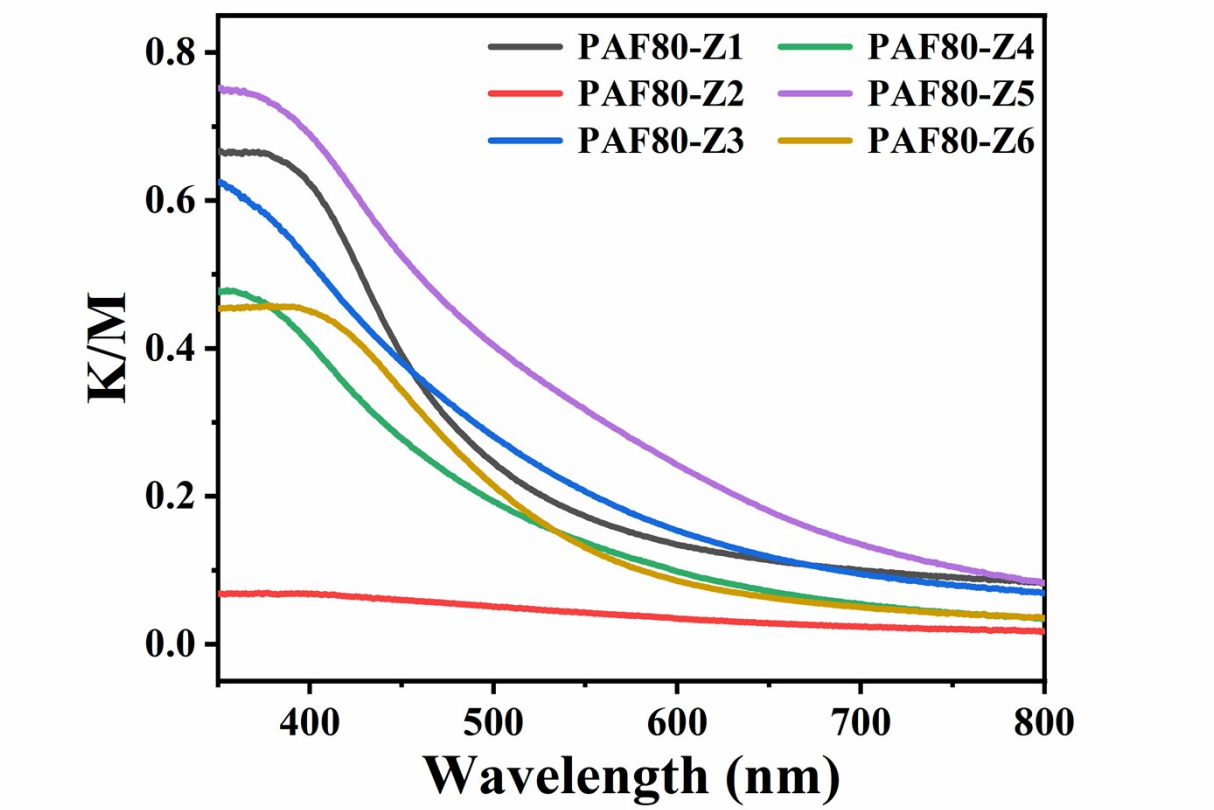

Fig. S7 Solid UV-Vis diffuse reflectance spectroscopy (sUV-Vis DRS) of PAF80-Z1 (black curve), Z2 (red curve), Z3 (blue curve), Z4 (green curve), Z5 (purple curve), Z6 (brown curve).

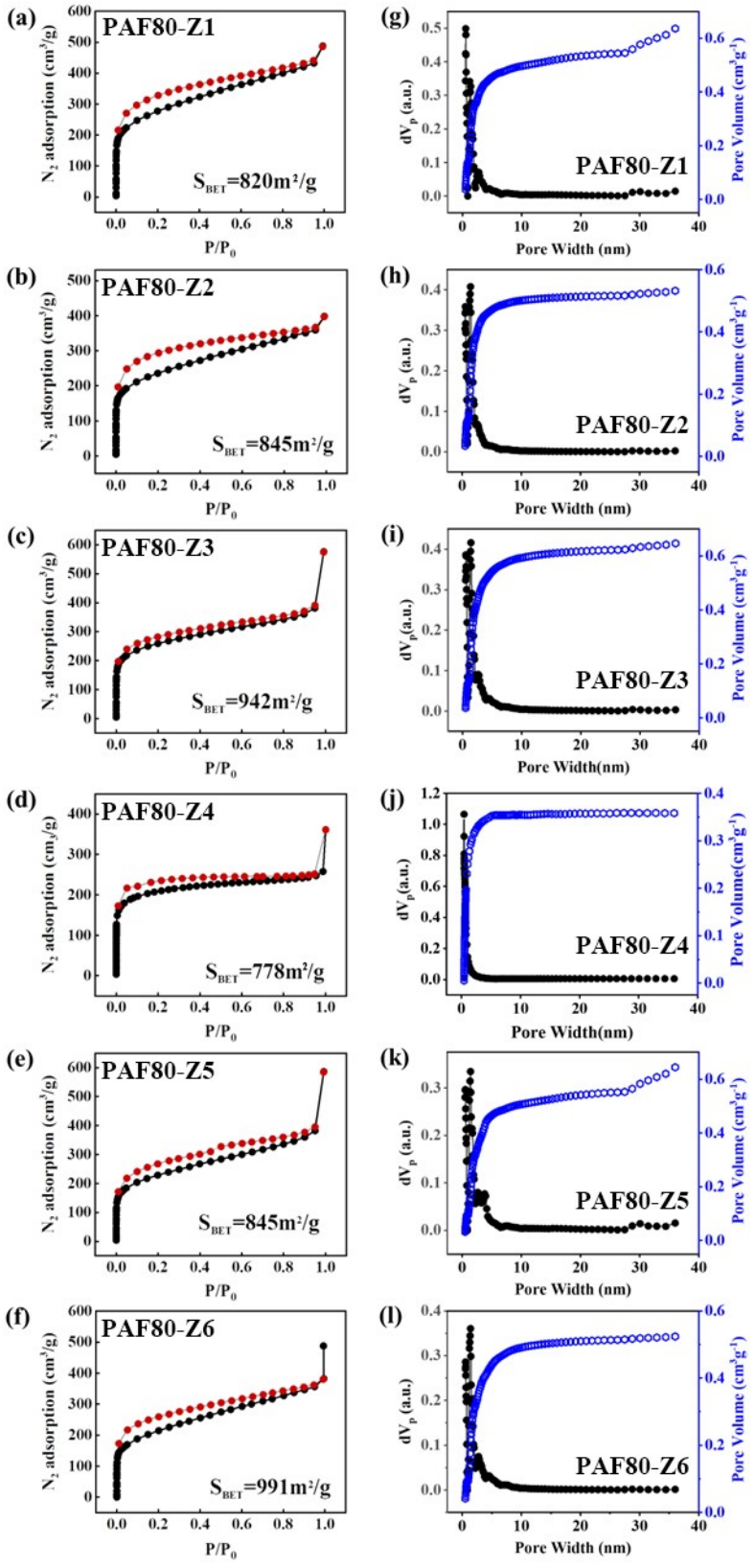

Fig. S8 Reversible nitrogen gas adsorption isotherms measured at 77 K, STP, and pore size distribution (PSD) profile of the PAF80-Z1~6 calculated via the NL-DFT method.

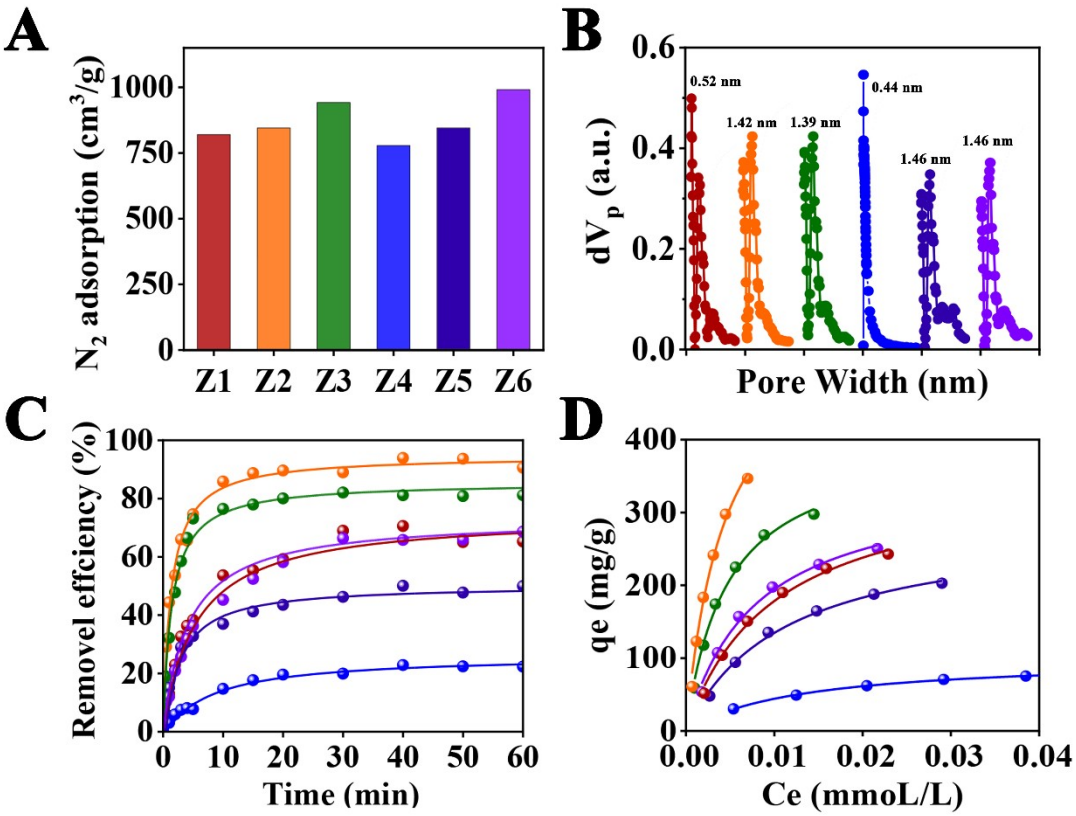

Fig. S9 (A) Histogram of specific surface area, (B) point line diagram of hole width, (each cell of the horizontal coordinate is from 0 to 5 nm), (C) kinetic binding profiles and (D) thermodynamic adsorption isotherms. In (B) to (D), PAF80-Z1 (red), Z2 (orange), Z3 (green), Z4 (blue), Z5 (dark blue), Z6 (purple).

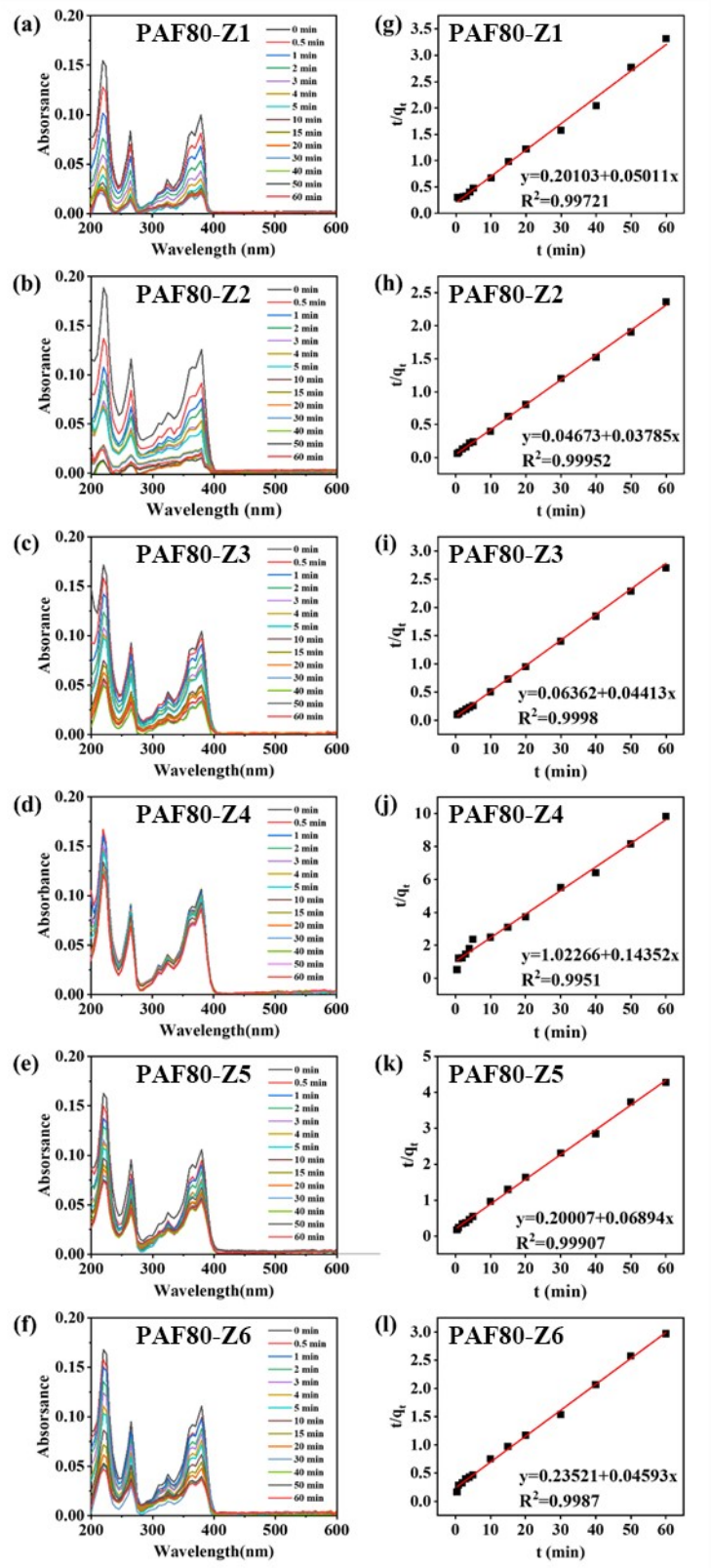

Fig. S10 Diagram of kinetic adsorption experiment of the PAF80-Z (1–6). (a) - (f) On the left is the ultraviolet absorption spectrum of SN-38's ultraviolet absorption intensity with adsorption time and (g) - (l) on the right is the removal efficiency curve.

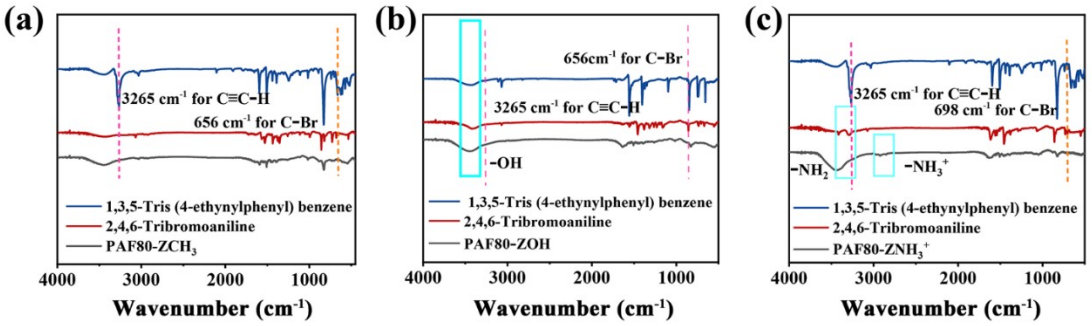

Fig. S11 FT-IR spectra of PAF80-Z2-(CH_3, OH, NH_3^+). The sharp peak at 3265 cm^{-1} belongs to the stretching vibration of alkyne hydrogen in the structural unit containing the acetylene functional group, the absorption peak near 656 cm^{-1} is the stretching vibration of C-Br in the monomer, and the disappearance of these characteristic peaks proves that the monomer has completely reacted. The broad absorption peak located at 3450 cm^{-1} is the stretching vibration of -OH in the structural unit, and the double absorption peak at 2800-3000 cm^{-1} is the stretching vibration of -NH_3^+ in the structural unit, which indicates that the hydroxyl and ammonium salts are retained after the reaction.

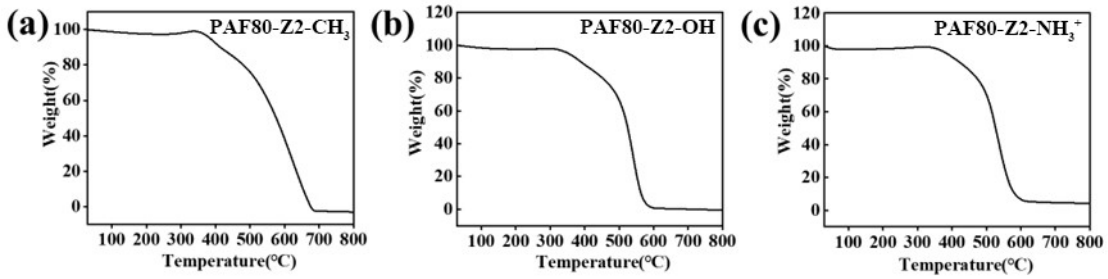

Fig. S12 TGA curves of PAF80-Z2-(CH_3, OH, NH_3^+). The thermal stability of the synthesized PAF materials up to 400 °C was shown by the TGA curves and no residues were observed above 800 °C.

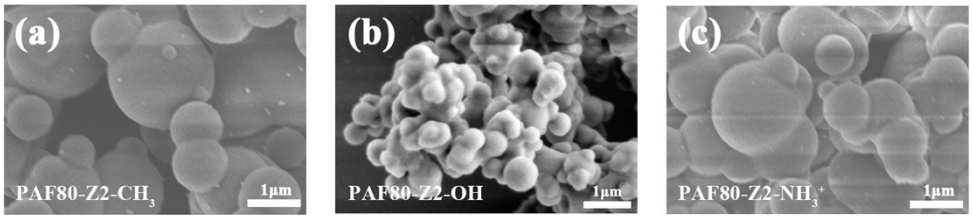

Fig. S13 SEM images of PAF80-Z2-(CH_3, OH, NH_3^+). The SEM images show they are submicron particles and spherical distribution.

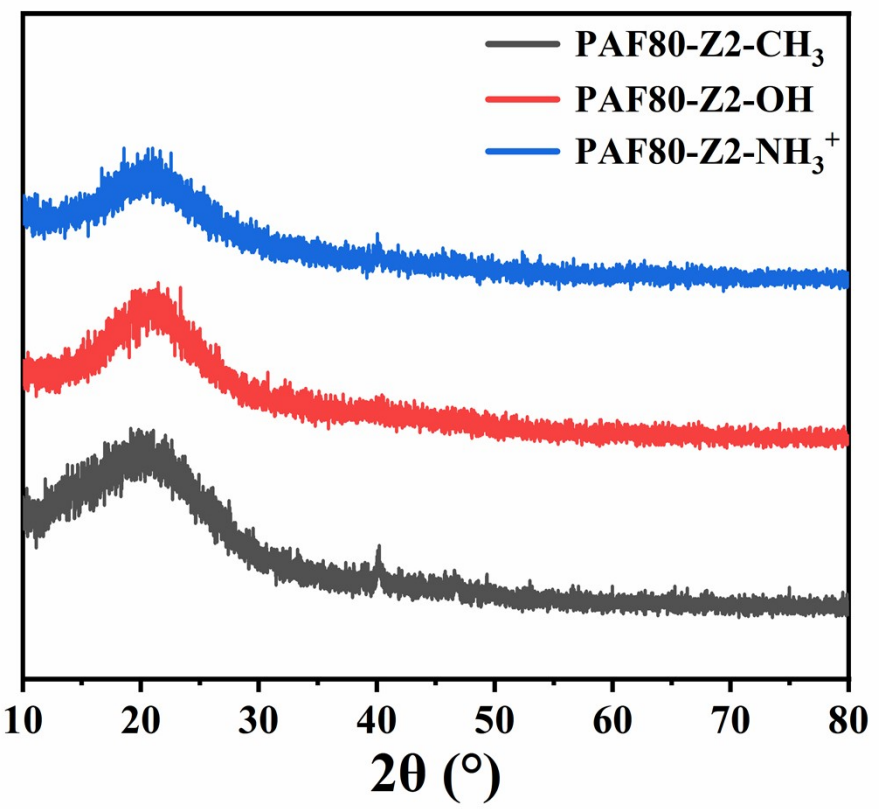

Fig. S14 PXRD patterns of PAF80-Z2-CH_3 (black curve), PAF80-Z2-OH (red curve), and PAF80-Z2-NH_3^+ (blue curve). As shown in PXRD patterns, all PAF materials are amorphous, probably because of the distortion and interpenetration of the aromatic fragments.

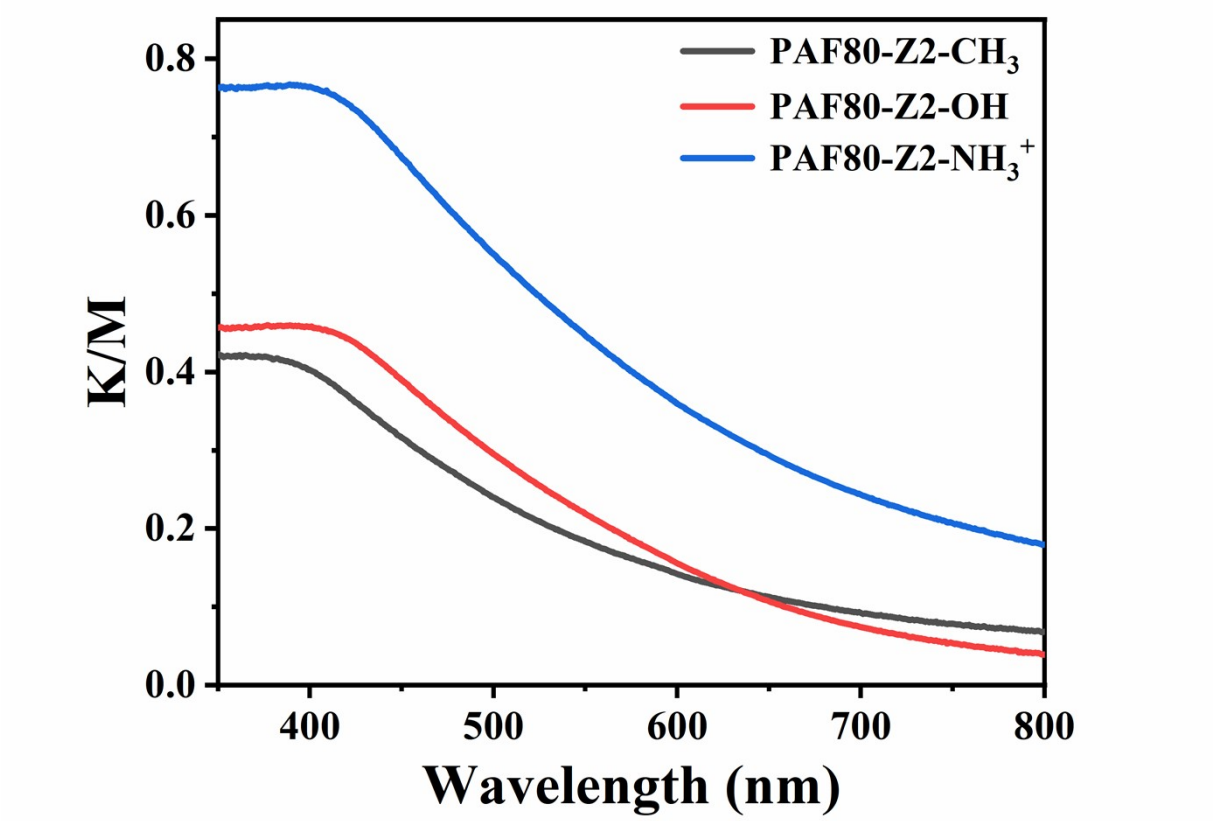

Fig. S15 sUV-Vis DRS of PAF80-Z2-CH_3 (black curve), PAF80-Z2-OH (red curve), and PAF80-Z2-NH_3^+ (blue curve).

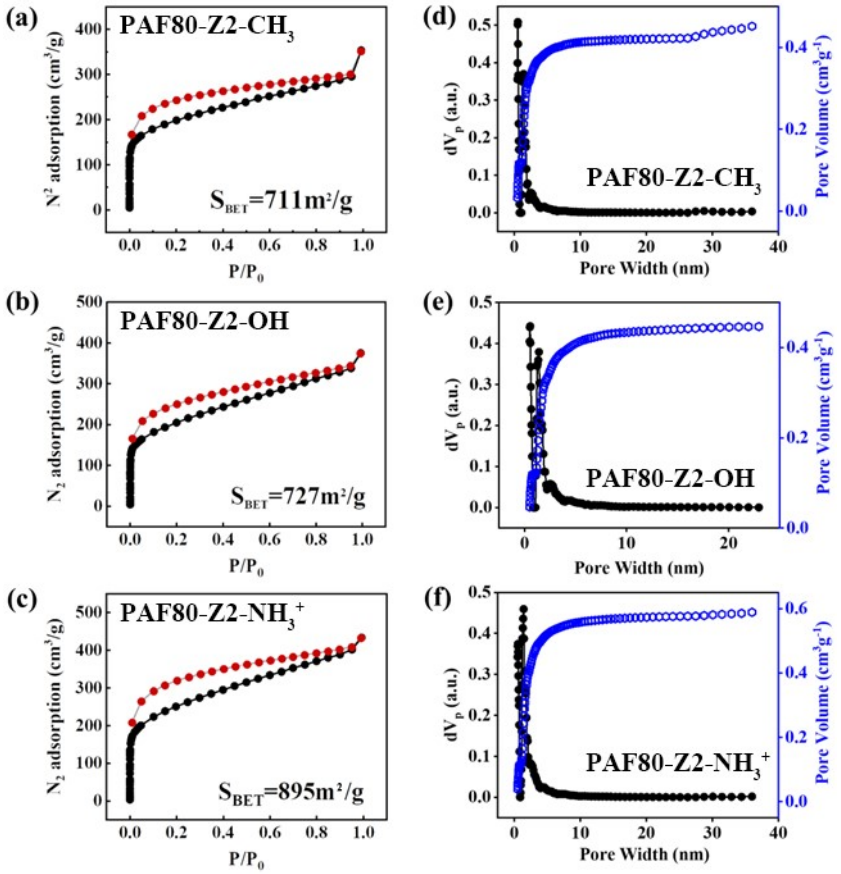

Fig. S16 Reversible nitrogen gas adsorption isotherms measured at 77 K, STP, and pore size distribution (PSD) profile of the PAF80-Z2-CH_3, PAF80-Z2-OH, PAF80-Z2-NH_3^+ calculated via the NL-DFT method. Black and red are abbreviations of adsorption and desorption.

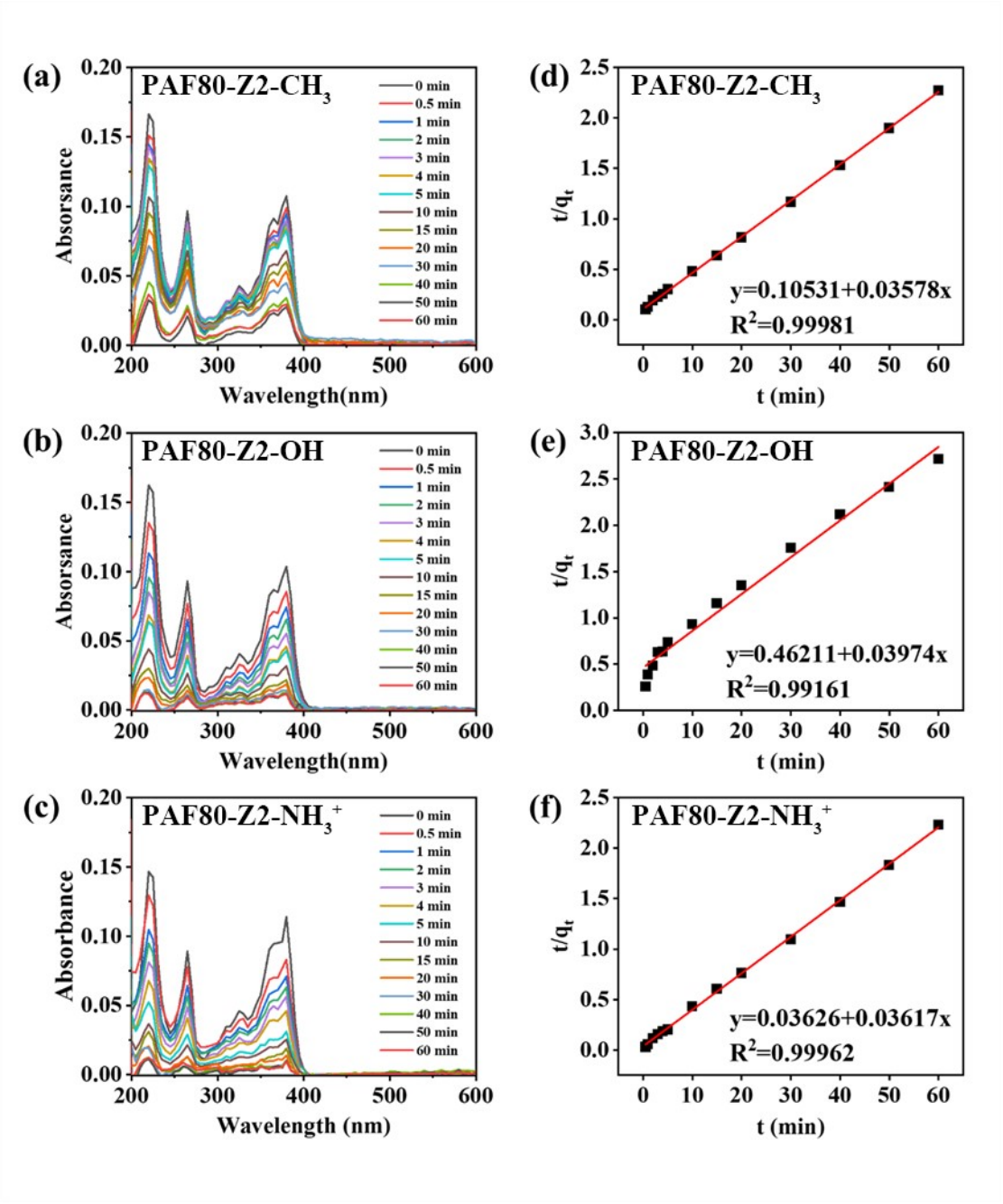

Fig. S17 Diagram of kinetic adsorption experiment of the PAF80-Z2-(CH_3, OH, NH_3^+). (a) - (c) The UV absorption spectrum of SN-38 with respect to adsorption time, and (d) - (f) the removal efficiency curve.

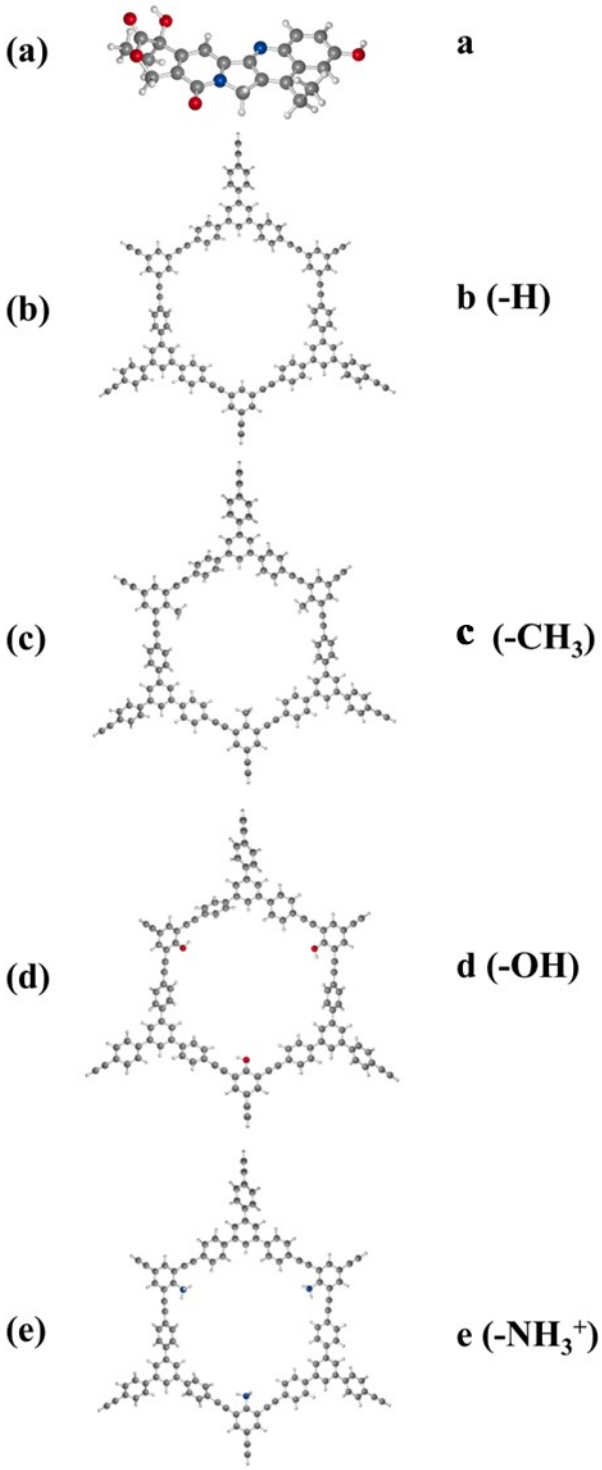

Fig. S18 Ball-and-stick model of each substance and their corresponding abbreviations named after functional groups

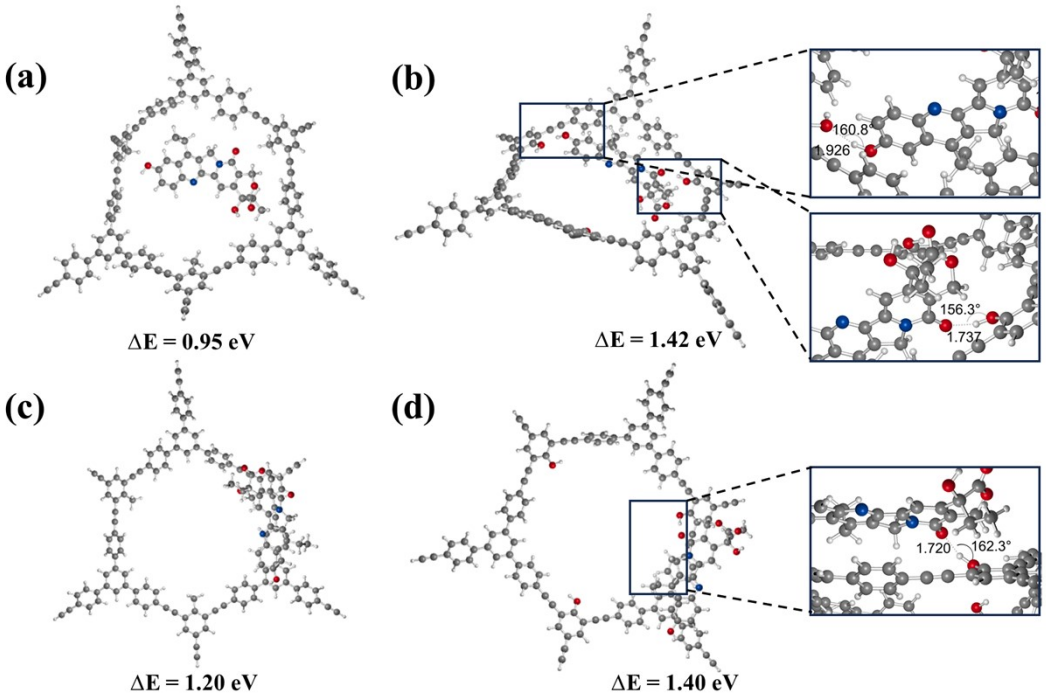

Fig. S19 (a) CPT-11 in the ring of PAF80-Z2-CH_3, (b) CPT-11 in the ring of PAF80-Z2-OH, (c) CPT-11 on the ring of PAF80-Z2-CH_3, and (d) CPT-11 on the ring of PAF80-Z2-OH.

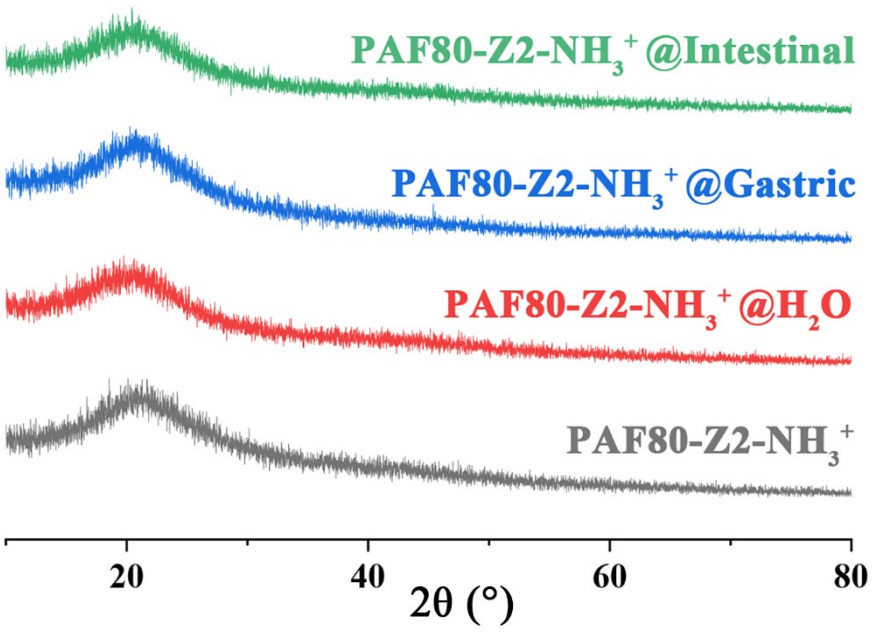

Fig. S20 PXRD patterns of PAF80-Z2-NH_3^+ before and after treated with H_2O (24 h at rt), gastric (HCl, pH = 1.2 at 37 ºC for 2 h), and intestinal conditions (ringer media pH = 6.0 at 37 ºC for 24 h). The PAF80-Z2-NH_3^+ is stable under GI conditions since their PXRD patterns are not affected after treatment.

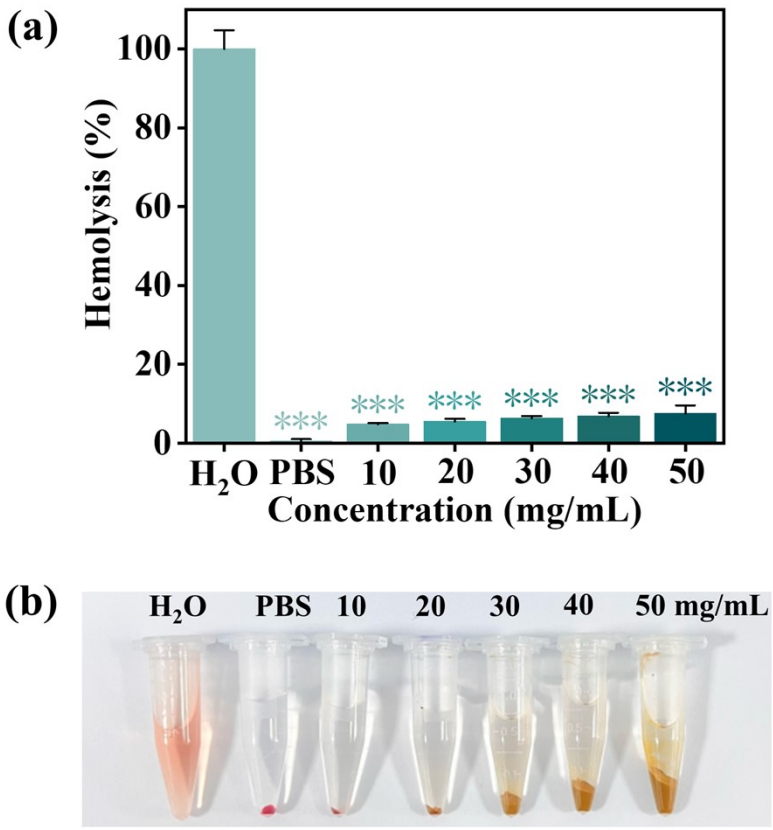

Fig. S21 Evaluation of the hemolysis effect by different concentrations of the PAF80-Z2-NH_3^+, (a) the supernatant obtained after incubating the PAF80-Z2-NH_3^+ in diluted fresh red blood cells, (b) hemolysis rate due to different concentrations of PAF80-Z2-NH_3^+. As in vitro hemolysis assay is a reliable and effective method to prove the hemocompatibility of nanomaterials, we performed in vitro hemolysis assay using 4% fresh blood from mice, as There is no hemolysis occurred at all the concentrations, which indicated that PAF80-Z2-NH_3^+ was not hemolyzed in the in vitro assay and was hemocompatible.

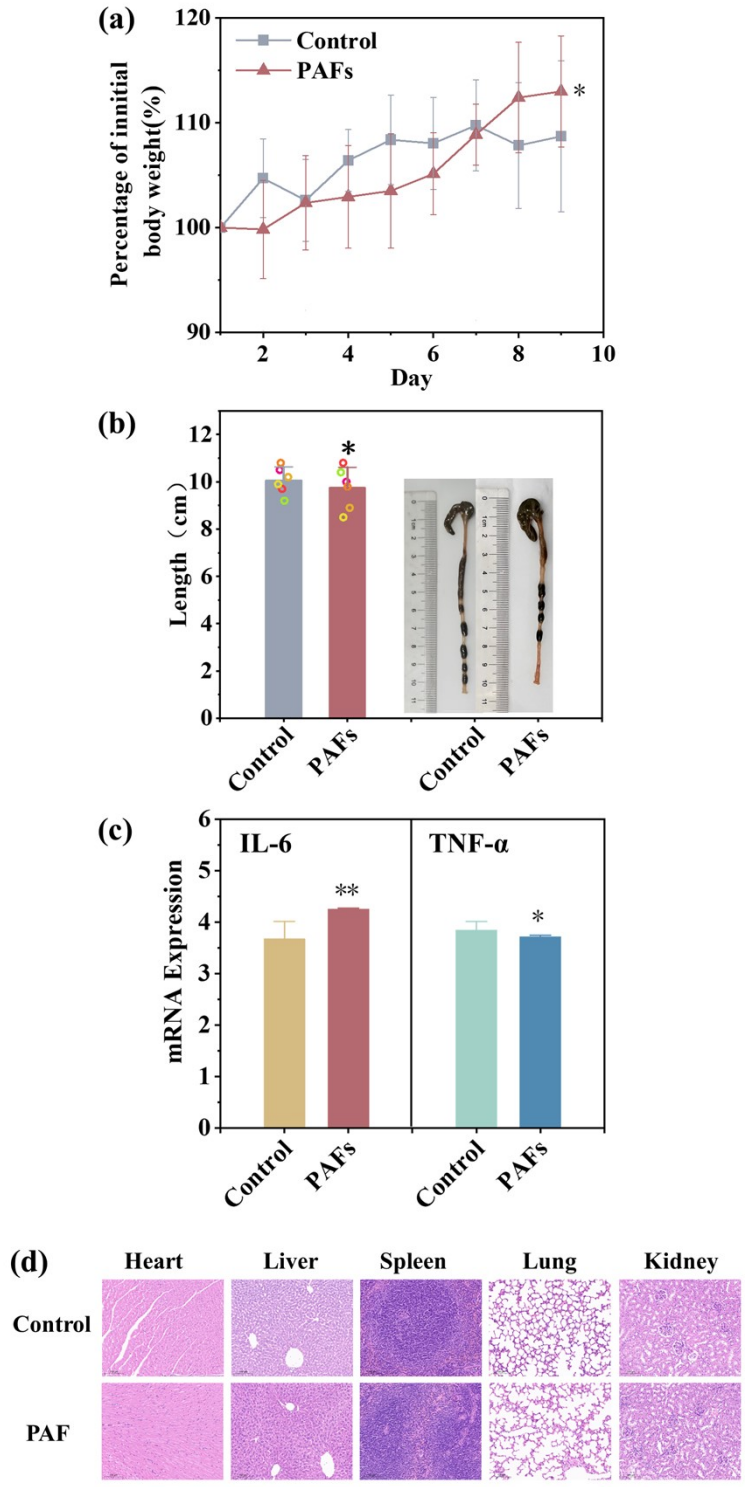

Fig. S22 The biological toxicity tests of PAF80-Z2-NH_3^+. (a) Trends in body weight of mice, (b) morphology and length of mouse colon, (c) serum levels of inflammatory factors (IL-6 and TNF-α) of mice, and (d) HE slices of heart, liver, spleen, lung, and kidney of mice.

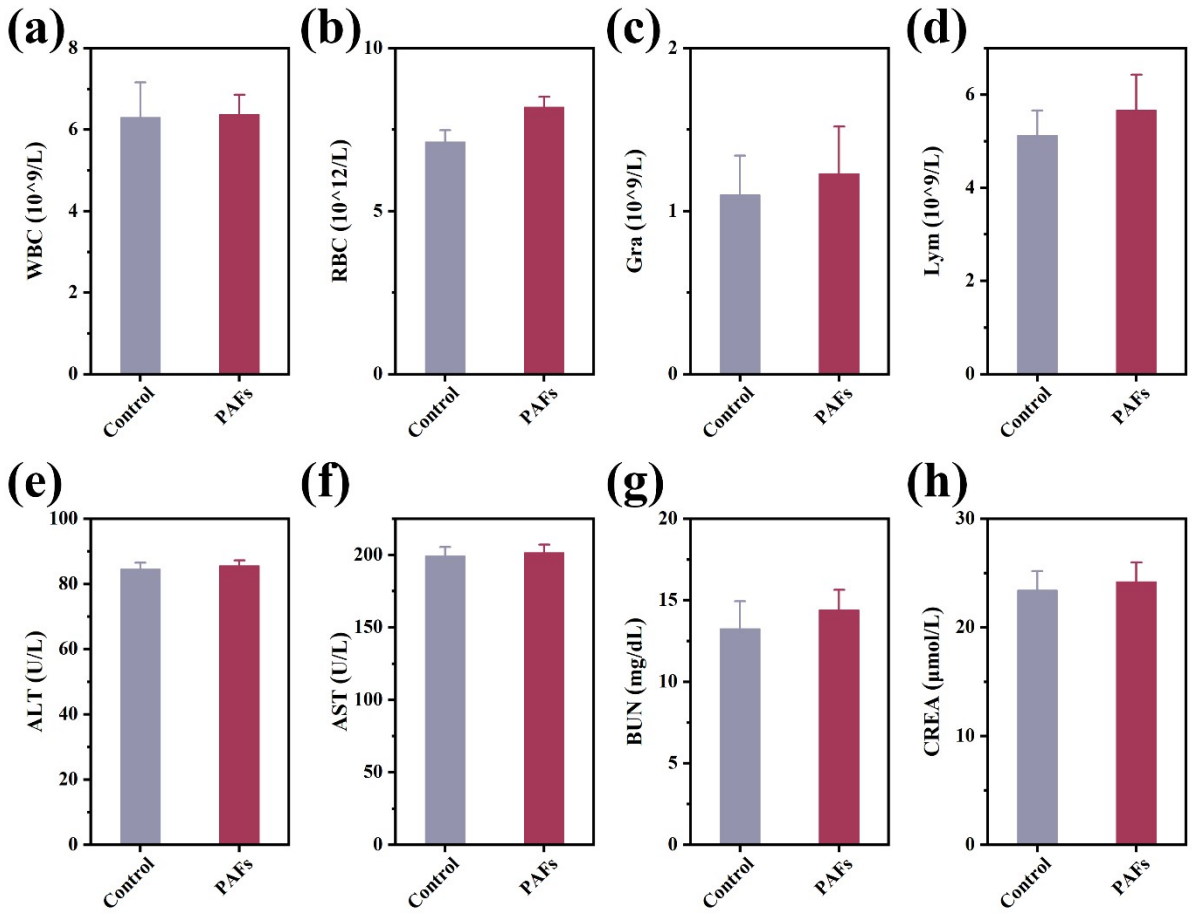

Fig. S23 (a-d) Serum biochemical indices for evaluating hematological parameters (WBC, RBC, Gra and Lym). Data are represented as mean ± SD. (e&f) Serum biochemical indices for evaluating liver function (ALT, AST). Data are represented as mean ± SD. (g&h) Serum biochemical indices for evaluating kidney function (BUN, CREA). Data are represented as mean ± SD.

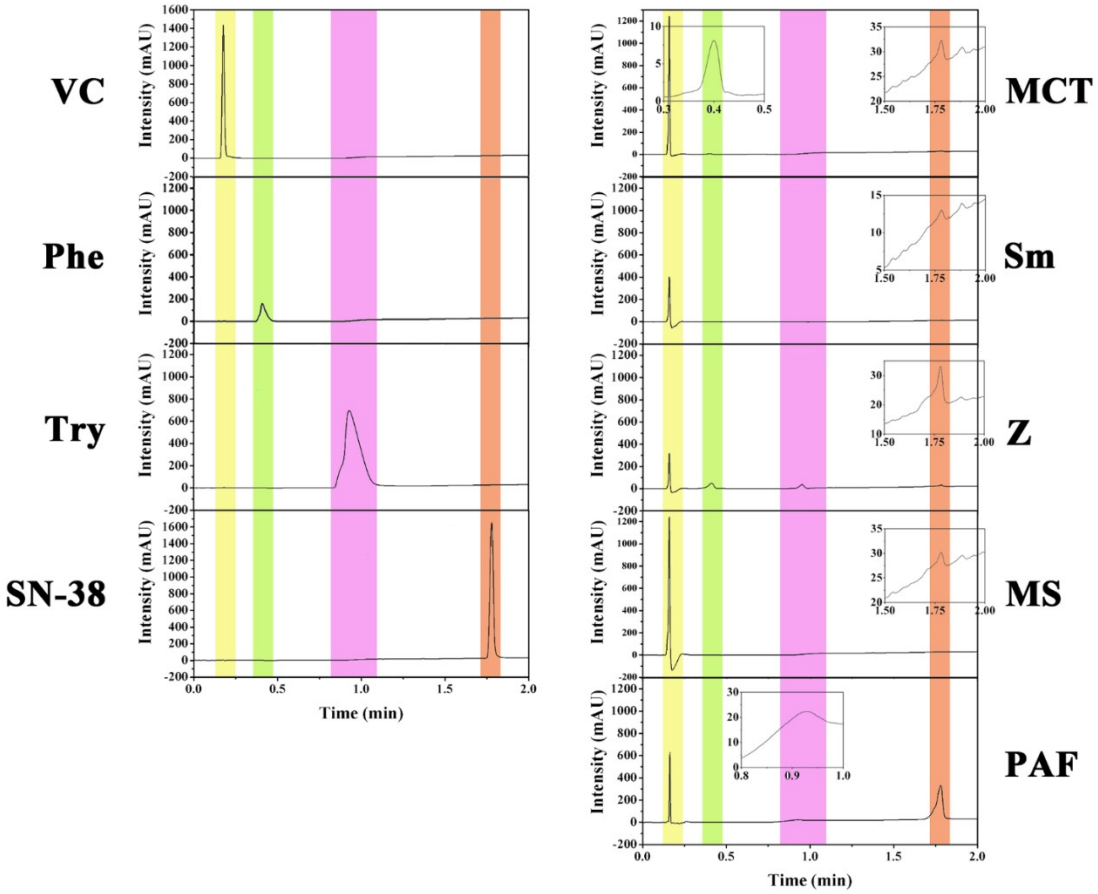

Fig. S24 Evaluating the adsorption selectivity of PAF80-Z2-NH_3^+ in complex systems using High Performance Liquid Chromatography (HPLC). Left Column: standard spectra of four substrates. Right Column: adsorption spectra after desorption of adsorbed substances from five porous materials following adsorption in complex systems. MCT: medicinal charcoal tablets; Sm: smectite powder; Z: ZIF-8; MS: mesoporous silica; PAF: PAF80-Z2-NH_3^+. Insert images were the partially enlarged images.

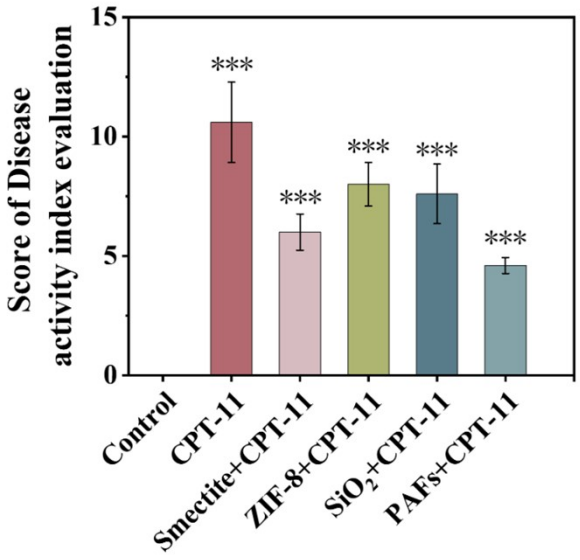

Fig. S25 Histogram of scores of disease activity index evaluation for each group of mice. SiO_2: mesoporous silicon.

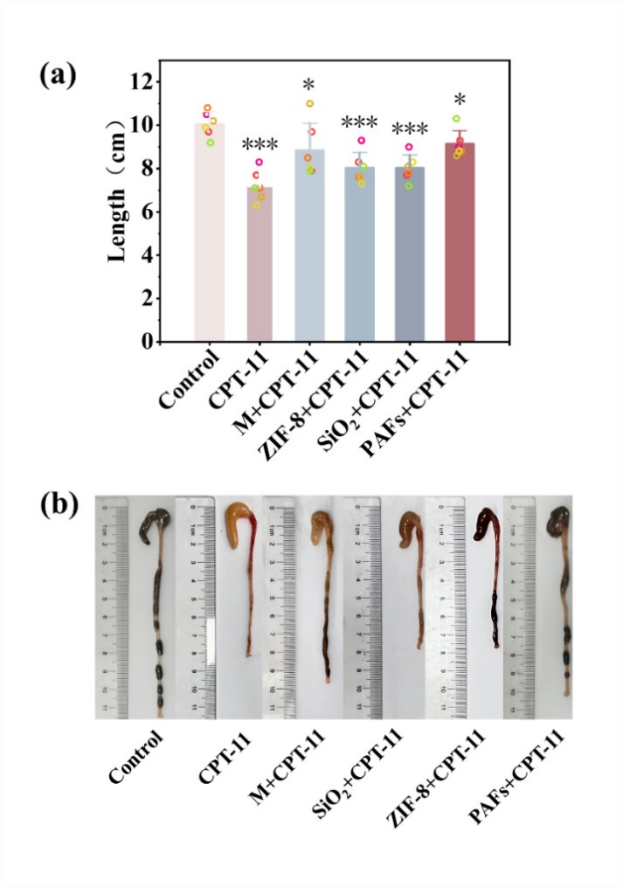

Fig. S26 (a) Histogram of the average colon length in each group of mice, (b) representative photographs of the colon in each group of mice. M: Smectite powder; SiO_2: mesoporous silicon.

Table S1 Animal experimental design diagram.

Group name	Methods
Control group	Normal diet
CPT-11 group	*i.p.* CPT-11
PAFs group	*i.g.* PAF80-Z2-NH_3^+
PAFs + CPT-11 group	*i.p.* CPT-11 + *i.g.* PAF80-Z2-NH_3^+
ZIF-8 + CPT-11 group	*i.p.* CPT-11 + *i.g.* ZIF-8
Mesoporous silica + CPT-11 group	*i.p.* CPT-11 + *i.g.* mesoporous silica
Smectite power + CPT-11 group	*i.p.* CPT-11 + *i.g.* MTSS

Each mouse was injected with H22 cell suspension (0.2 mL, 10^6 cells/mL) in the axilla on day 0, and the tumor was eligible for subsequent experiments on day 5. 9-day experiment was performed from day 6 to day 14, with specific grouping and experimental manipulations as shown in Table S2. Dissection was performed on day 14, and the tumors were weighed and the volume of the tumors was measured. The concentrations of the reagents used in the experiment were as follows CPT-11 injection was 10 mg mL^{-1} and the detoxifying agents was a suspension of 30 μg mL^{-1}. The irinotecan dosage for low dose groups was 50 mg kg^{-1}, the irinotecan dosage for medium dose groups was 75 mg kg^{-1}, The irinotecan dosage for high dose groups was 100 mg kg^{-1}. The PAF80-Z2-NH_3^+ dosage for every mouse was 200 mg kg^{-1}.[1]

Table S2 Animal experimental design diagram.

Group name	Methods
Control group	Normal diet
High dose CPT-11	*i.p.* 50 mg kg^{-1} CPT-11
Medium dose CPT-11	i.g. 75 mg kg^{-1} CPT-11
Low dose CPT-11	*i.p.* 100 mg kg^{-1} CPT-11
High dose CPT-11 + PAF	*i.p.* 50 mg kg^{-1} CPT-11 + *i.g.* 200 mg kg^{-1} PAF80-Z2-NH_3^+
Medium dose CPT-11 + PAF	*i.p.* 75 mg kg^{-1} CPT-11 + *i.g.* 200 mg kg^{-1} PAF80-Z2-NH_3^+
Low dose CPT-11 + PAF	*i.p.* 100 mg kg^{-1} CPT-11 + *i.g.* 200 mg kg^{-1} PAF80-Z2-NH_3^+

Table S3 Scoring criteria for body weight, diarrhea, and occult blood in the stool.

Point	Diarrhea score	Blood in the feces	Body weight loss (%)
0	Normal	No blood (−)	No loss
1	Loose stool (slight, slightly wet and soft stool)	Positive (+)	1–5%
2	Watery diarrhea (wet and unformed stool with moderate perianal staining of the coat)	Positive (++)	5%–10%
3	Slimy diarrhea	Positive (+++)	10%–15%
4	Severe watery diarrhea with blood	Positive (++++) or visible bleeding	over 15%

Table S4 Scoring criteria for body weight, diarrhea, and occult blood in the stool.

Evaluation Parameters	Score	Feature Description
Inflammation	0	Normal, no inflammation
	1	Mild inflammation
	2	Moderate inflammation
	3	Severe inflammation with marked inflammatory cell infiltration and extensive separation of glands
Mucosal injury	0	Normal
	1	Damage limited to the mucosal layer
	2	Injury penetrates deep into the submucosa
	3	Injury penetrates into the basal and mucosal layers
Degree of glandular damage	0	Normal
	1	Minimal, small amount of glandular dilatation
	2	Mild, multifocal glandular dilatation
	3	Moderate, multifocal glandular dilatation with glandular disappearance
Affected area	0	None
	1	Small amount: <10%
	2	Mild: 10-25%
	3	Moderate: 26-50%
	4	Significant: >50%

Table S5 Ho and McKay fitted a secondary adsorption model of SN-38 and PAF80-Z (1-6).

	Kobs (g mg^{-1}·min)	Equation	Correlation coefficient (R^2)
PAF80-Z1	0.0125	y=0.20130+0.05011x	0.9972
PAF80-Z2	0.0307	y=0.04673+0.03785x	0.9995
PAF80-Z3	0.0306	y=0.06362+0.04413x	0.9998
PAF80-Z4	0.0201	y=1.02266+0.14352x	0.9951
PAF80-Z5	0.0238	y=0.20007+0.06894x	0.9991
PAF80-Z6	0.009	y=0.23521+0.04593x	0.9987

Table S6 Langmuir adsorption linear models of SN-38 and PAF80-Z (1-6).

	Qmax (mg g^{-1})	K (L $mmol^{-1}$)	Equation	Correlation coefficient (R^2)
PAF80-Z1	347	127	y=44069x/(1+127x)	0.9906
PAF80-Z2	576	226	y=130176x/(1+226x)	0.9901
PAF80-Z3	402	213	y=85626x/(1+213x)	0.9910
PAF80-Z4	100	78	y=7800x/(1+78x)	0.9992
PAF80-Z5	285	88	y=25080x/(1+88x)	0.9925
PAF80-Z6	357	99	y=35342x/(1+99x)	0.9916

Table S7 Ho and McKay fitted secondary adsorption model of SN-38 and PAF80-Z2, PAF80-Z2-CH_3, PAF80-Z2-OH, and PAF80-Z2-NH_3^+.

	Kobs (g mg^{-1}·min)	Equation	Correlation coefficient (R^2)
PAF80-Z2	0.0307	y=0.04673+0.03785x	0.9995
PAF80-Z2-CH_3	0.0122	y=0.10531+0.03578x	0.9998
PAF80-Z2-OH	0.0397	y=0.46211+0.03974x	0.9916
PAF80-Z2-NH_3^+	0.0361	y=0.03636+0.03617x	0.9996

Table S8 Langmuir adsorption linear models of SN-38 and PAF80-Z2, PAF80-Z2-CH_3, PAF80-Z2-OH, and PAF80-Z2-NH_3^+.

	Qmax (mg g^{-1})	K (L $mmol^{-1}$)	Equation	Correlation coefficient (R^2)
PAF80-Z2	576	226	y=130176x/(1+226x)	0.9901
PAF80-Z2-CH_3	534	218	y=116412x/(1+218x)	0.9939
PAF80-Z2-OH	604	216	y=130464x/(1+216x)	0.9925
PAF80-Z2-NH_3^+	677	225	y=152325x/(1+225x)	0.9899

Table S9 Energetic information for each substrate, drug molecule, and substrate-drug molecule (A and B denote two binding sites of CPT-11 molecules to the porous aromatic framework structure, with A located inside the ring of the substrate molecule and B located on the ring of the substrate molecule).

material	Single point Energy A (hartree)	Binding Energy A (hartree)	Binding Energy A (eV)	Single point Energy B (hartree)	Binding Energy B (hartree)	Binding Energy B (eV)
A	-1336.146227					
b (-H)	-4379.840687					
c (-CH_3)	-4497.763984					
d (-OH)	-4605.589739					
e (-NH_3^+)	-4546.891214					
b (-H)-a	-5716.021633	-0.034719	-0.94470399	-5716.029836	-0.042922	-1.16790762
c (-CH_3)-a	-5833.944991	-0.03478	-0.9463638	-5833.954183	-0.043972	-1.19647812
d (-OH)-a	-5941.788067	-0.052101	-1.41766821	-5941.787278	-0.051312	-1.39619952
e (-NH_3^+)-a	-5883.108919	-0.071478	-1.94491638	-5883.119696	-0.082255	-2.23815855

Table S10 Adsorption mass of five porous materials for four substrates (unit: mg) (MCT: medicinal charcoal tablets; Sm: smectite powder; Z: ZIF-8; MS: mesoporous silica; PAF: PAF80-Z2-NH_3^+.).

	Vc	Phe	Tyr	SN-38
Control	0.141	0.132	0.163	0.314
MCT	0.128	0.00743	0	0.0497
Sm	0.0435	0	0	0.0198
Z	0.0342	0.0477	0.00274	0.0240
MS	0.145	0	0	0.0478
P	0.0525	0	0.00582	0.287

Table S11 Removal efficiency of five porous materials for four substrates (unit: %) (MCT: medicinal charcoal tablets; Sm: smectite powder; Z: ZIF-8; MS: mesoporous silica; PAF: PAF80-Z2-NH_3^+.).

	Vc	Phe	Tyr	SN-38
MCT	90.50	5.63	0	15.84
Sm	30.89	0	0	6.30
Z	24.24	36.06	1.68	7.66
MS	102.68	0	0	15.23
P	37.28	0	3.56	91.38

3. Reference

1 L. Wang, R. Wang, G. Y. Wei, R. P. Zhang, Y. Zhu, Z. Wang, S. M. Wang, G. H. Du, *Pharmacol. Res.* 2021, **163**, 105232.